Metal-based nanorods as molecule-specific contrast agents for reflectance imaging in 3D tissues

David J. Javier,[a] Nitin Nitin,[b] Darren M. Roblyer,[c] Rebecca Richards-Kortum[d]
Department of Bioengineering, Rice University, 6100 Main St., Keck Hall 116, Houston, TX 77054
djj3872@rice.edu,[a] nn3995@rice.edu,[b] dmr2@rice.edu,[c] rkortum@rice.edu[d]

Abstract. Anisotropic metal-based nanomaterials have been proposed as potential contrast agents due to their strong surface plasmon resonance. We evaluated the contrast properties of gold, silver, and gold-silver hybrid nanorods for molecular imaging applications in three-dimensional biological samples. We used diffuse reflectance spectroscopy to predict the contrast properties of different types of nanorods embedded in biological model systems of increasing complexity. The predicted contrast properties were then validated using wide-field and high-resolution imaging. Results demonstrated that silver nanorods yield images with higher positive-contrast than gold nanorods; however, it is more difficult to synthesize silver nanorods which are homogeneous in shape and size. Gold-silver hybrid nanorods combine the homogeneous synthesis of gold nanorods with the higher scattering properties of silver nanorods. The spectroscopic and imaging results demonstrated that the image contrast properties that can be achieved with anisotropic nanomaterials depend strongly on the material composition, mode of imaging, presence of targeting molecules, and the biological environment. We also found that gold, silver, and gold-silver hybrid nanorods are stable and biocompatible sources of positive and absorptive contrast for use in reflectance molecular imaging and are promising for future clinical translation.

Keywords: metal nanorods, molecule-specific contrast agents, diffuse reflectance spectroscopy, wide-field imaging, high-resolution imaging.

1 INTRODUCTION

The field of molecular imaging relies on the development of targeted contrast agents that bind to disease specific biomarkers in vivo and result in good image contrast between labeled and unlabeled tissue. Recently, there has been a significant interest in developing contrast agents based on metal nanoparticles to improve sensitivity of detection for optical imaging applications. A variety of metal nanoparticles have been synthesized with different material compositions, each providing unique spectral signatures for biological imaging applications. For example, gold and silver nanoparticles have been utilized for reflectance-based spectroscopy or imaging due to their strong localized surface plasmon resonance [1, 2]. The potential use of gold nanoparticles as molecule-specific contrast agents has been demonstrated for cancer diagnostics [3, 4]. Ideally, molecule-specific metal nanoparticles targeted against appropriate biomarkers should increase the contrast in reflectance between diseased and normal tissue.

The resulting image contrast between labeled and unlabeled tissue depends on the nature of the particles (size, material composition, geometry), the properties of the target tissue (baseline optical properties, targeted biomarker concentration) and the properties of the imaging system (imaging mode, illumination wavelength, magnification, numerical aperture). Maximizing image contrast for a particular application requires an understanding of the interplay of these factors. In a previous study, we developed an approach to systematically

Received 4 Jan 2008; accepted 14 Apr 2008; published 23 Apr 2008 [CCC: 19342608/2008/$25.00]

evaluate the contrast properties of gold and silver nanospheres using high-resolution and wide-field imaging modalities for model tissues [5]. Results suggested that both native tissue reflectance and the type of imaging modality influence the resulting image contrast of three-dimensional (3D) tissues labeled with metal nanospheres. In order to translate these agents to clinical application, it is important to optimize properties of nanoparticles in order to maximize contrast and achieve a clinically meaningful difference. For wide-field imaging applications, an increase of contrast ratios of 1.5 to 3.0 units is considered significant [6-8].

Metal nanorods offer several advantages over nanospheres for optical reflectance imaging [9]. First, metal nanorods have been shown to have higher scattering properties compared to metallic nanospheres due to their anisotropic structure [10]. Second, the reflectance spectra of metallic nanorods have peaks at longer wavelengths (570 to 670 nm range) compared to metal nanospheres (430 to 530 nm range), allowing deeper light penetration and improved collection of scattered light in tissue samples. The goal of this study is to evaluate contrast that can be achieved using nanorod-based contrast agents for molecular imaging in model 3D tissue systems.

However, there are several challenges in the use of nanorod-based contrast agents. The synthesis of metallic nanorods involves use of surfactants that can affect the stability, biocompatibility, and bioconjugation of these materials [11]. Surfactant-coated nanoparticles are not stable in physiological buffers. In order to stabilize them, these materials must be coated with polymers to prevent aggregation. A study by the Caruso group has shown that charged polymers such as PSS and PDADMAC can improve the stability of the nanomaterials in physiological environments [12]. The use of polymeric coatings also protects cells from exposure to the surfactant layer to avoid any cytotoxic effects in biological samples. Thus, polymer coating can potentially improve the biocompatibility of anisotropic nanomaterials for biological imaging.

Another challenge in the development of molecule-specific contrast agents using anisotropic materials is the conjugation of targeting molecules to the surface of the nanomaterials. Various chemical and physical approaches have been proposed to link biomolecules to the surface of such nanomaterials. For chemical-conjugation approaches, introduction of specific bifunctional polymers such as PEG-thiol with NHS ester have been used to introduce biomolecules via gold-sulfur interactions [13]. A limitation of this approach is that it requires displacement of the surfactant molecules to allow the sulfur groups to intercalate on the gold lattice. The gold-sulfur interaction is predominantly favored in areas with low surfactant coverage (e.g. the transverse ends of gold nanorods). The displacement process can potentially lead to instability and it is often difficult to achieve complete displacement. As an alternative, physical methods using electrostatic interactions between the targeting proteins and the polymeric coating have been proposed to allow conjugation of antibodies on gold nanorods. This method overcomes the limitations associated with chemical displacement as the surfactant layer is maintained due to deposition of polymeric coatings.

To develop optimized contrast agents for reflectance imaging in tissue samples, it is necessary to consider their contrast properties together with issues concerning stability, biocompatibility, and bioconjugation. In this study, we develop anisotropic molecule-specific, biocompatible contrast agents with optimal material composition to enhance contrast for reflectance imaging in biological matrices. We compare the image contrast that can be achieved using gold, silver, and gold-silver hybrid nanorods. We use reflectance spectroscopy to predict the anticipated image contrast properties of nanorods in various biological models. These predictions are then validated using wide-field and high-resolution imaging.

2 MATERIAL AND METHODS

2.1 Materials

High-purity (>99%) chemicals for nanoparticle synthesis, including cetyltrimethylammonium bromide (CTAB), poly(vinylpyrrolidone) (PVP) sodium borohydride ($NaBH_4$), sodium citrate, ascorbic acid, gold chloride ($HAuCl_4$), silver nitrate ($AgNO_3$), and sodium hydroxide (NaOH) were purchased from Sigma-Aldrich. Specifically, $HAuCl_4$ and $AgNO_3$ were purchased from Sigma with >99.999% purity and stored in the dark under desiccating conditions. For coating of nanoparticles, poly(styrenesulfonate), M_w ~15,000 (PSS) was purchased from Polysciences, Inc.

In this study, the SiHa cervical cancer cell line was used as a model system to test contrast agents targeted against the epidermal growth factor receptor (EGFR). The SiHa cell line was purchased from ATCC and cultured using recommended media and conditions. Specifically, DMEM (Dulbecco's minimum essential media) with 5% FBS (Fetal Bovine Serum) with antibiotics was used. Nanoparticles were targeted using an anti-EGFR antibody (clone 29.1, Sigma) as positive control and an IgG antibody (clone UPC-10) as a negative control.

2.2 Methods

2.2.1 Synthesis, TEM, and UV-Vis analysis of metallic nanorods:

To synthesize gold nanorods, we adapted the procedure developed by the El-Sayed group [14]. A seed solution was developed by $NaBH_4$-mediated reduction of Au ions in presence of CTAB. This seed solution was added to a growth solution, which was prepared by mixing $AgNO_3$ and $HAuCl_4$ with CTAB followed by reduction with ascorbic acid. The CTAB solution was purified using a 100 nm filter (Millipore) to remove any CTAB aggregates after dissolution. These filters were pre-treated with water and CTAB before use. For the growth stage, $AgNO_3$ was sonicated for 2 min with CTAB solution to provide uniform mixing. A longer incubation time (overnight) was used to promote growth of nanorods and to enhance the uniformity in size and shape of the particles.

To synthesize silver nanorods, we used the procedure reported by the Murphy group [15]. Silver nanorods were formed by a two-step synthesis. In the first step, a seed solution was formed by reduction of $AgNO_3$ using sodium citrate and $NaBH_4$. Next, a growth solution was prepared by mixing $AgNO_3$ with CTAB and ascorbic acid. After aging the seed for 2 h, a fixed volume of seed solution was added to the growth solution. NaOH was added to change the pH and initiate the formation of silver nanorods. The process was monitored by observing the significant changes in color of the resulting growth solutions which are distinct for nanorods of different sizes.

To synthesize gold-silver hybrid nanorods, gold nanorods were initially synthesized according to the procedure outlined above. After a 24-h aging process, the gold nanorods were used as a template to deposit a layer of silver metal on the surface. This process was carried out by reduction of $AgNO_3$ in the presence of 1% PVP, ascorbic acid and gold nanorods. To trigger the deposition, NaOH was used to change the pH of the solution. The procedure for the development of the gold-silver core-shell hybrid materials was adapted from Guyot-Sionnest group [16].

After synthesis, the size of the gold, silver, and gold-silver hybrid nanorods was analyzed using transmission electron microscopy (JEOL1010 TEM). Samples were centrifuged once at 6000 rpm (3300 g) for 20 min to remove excess CTAB from the growth solution. After centrifugation, 2 μl solutions of resulting particles were deposited on carbon coated TEM grids and allowed to dry overnight.

UV-Vis analysis was also used to characterize the absorption spectra of the nanorods. For this analysis, particles were used as prepared without any centrifugation or other separation processes. The UV-Vis measurements were carried out from 350-800 nm using a Cary 50 spectrophotometer.

2.2.2 Biocompatibility of metallic nanorods

The biocompatibility of PSS coated nanorods was determined using the MTT assay following the procedure recommended by ATCC. Briefly, cells were cultured in 90-well plates for 24 h prior to incubation with gold, silver and gold-silver hybrid nanorods. In each experiment, three wells were incubated with each of the nanorods along with triplicate control wells. The experiment was carried out using the SiHa cervical cancer cell line. The concentration of coated nanorods (sub-nM range) was the same as that for cell labeling. After 24 h of incubation, the plates were assayed using reagents provided with the MTT kit. The absorbance at 570 nm associated with metabolic activity of cellular enzyme (mitochondrial reductase) was measured using a plate reader. The background level was determined using cells without any treatment and MTT reagents.

2.2.3 Conjugation of targeting agents with nanoparticles and high-resolution confocal imaging

To synthesize targeted nanorods, anti-EGFR antibodies were conjugated to the surface of the gold, silver, and gold-silver hybrid nanorods. The metal nanorods were first coated with PSS using methods adapted from the layer-by-layer deposition developed by the Caruso group [12]. This coating approach provided a negatively charged surface and also limited the direct exposure of CTAB which was cytotoxic. After PSS coating, antibodies were directly absorbed on the surface of the Au, Ag, and Au-Ag hybrid nanorods. The conjugation process was similar to the use of polyelectrolyte coatings reported by the Murphy group [17]. For efficient coating, PSS was incubated overnight with nanorods at a final concentration of 1 mg/ml in 1 mM NaCl. After PSS coating, nanorods were centrifuged to remove excess PSS and coated with antibodies for 30 min. Excess antibodies were removed by centrifugation at 6000 rpm (3300 g) for 20 min.

An aliquot of cells (>40 M cells/mL) was labeled with a solution of each type of anti-EGFR targeted nanorods at room temperature for 30 min. Labeled cells were imaged using standard confocal reflectance microscopy (LSM 510, Zeiss). The reflectance confocal imaging was carried using a 633 nm laser excitation and the reflected signal was collected using a 685 nm low pass filter, which allows detection of light scattered from the sample. The intensity of the reflectance signal from specifically labeled cells was compared to that measured from negative controls (cells incubated with an equal concentration of IgG-conjugated nanorods).

2.2.4 Diffuse reflectance spectroscopy

Diffuse reflectance spectroscopy was used to characterize the reflectance properties of various metal nanorods embedded in a variety of media including water, gelatin, and 3D cell culture (>40 million cells/ml). Reflectance spectra were measured using a Cary 5000 spectrophotometer equipped with an integrating sphere to collect backscattered light. To remove any contribution from specular reflection, the integrated sphere was set up to collect only diffusely scattered light. To prepare water and 3% gelatin phantoms with nanoparticles, a 3-fold dilution of a stock solution of nanoparticles (sub-nM concentration range) in water or gelatin was used. Measurements were obtained from 400-800 nm. Reflectance spectra of solution or gelatin containing nanoparticles were divided by spectra of an unlabeled control sample to calculate the change in reflectance intensity. For 3D cell culture, cells were labeled

with anti-EGFR conjugated nanoparticles at room temperature for 30 min. The labeled cells were centrifuged (800 x g for 1 min) and the resulting pellet was resuspended in 3% gelatin. A phantom containing unlabeled cells at the same concentration was used as a reference to calculate the relative change in reflectance intensity.

2.2.5 Wide-field imaging

A multispectral digital microscope (MDM) [18] was used to obtain wide-field reflectance images of the labeled and unlabeled gelatin and 3D cell culture. As shown in Fig. 1, the device captured images at a 25 cm working distance with a field of view that can vary from approximately 1 to 6 cm. Narrowband excitation filters centered at 450 nm, 530 nm, 600 nm, and 650 nm were used with a broadband lamp to illuminate samples and a scientific grade CCD camera was used to collect the images.

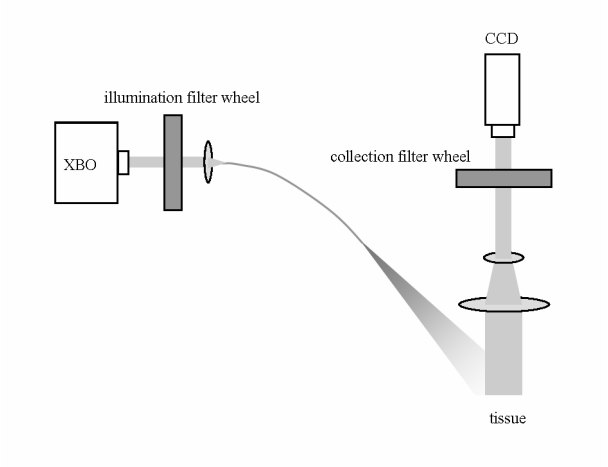

Fig. 1. Schematic representation of the multispectral digital microscope (MDM) used for wide-field imaging studies.

Gelatin and 3D cell culture were prepared as indicated above and imaged atop a black background. A central region of interest was selected from each sample and the mean reflectance intensity was calculated. Pure gelatin and unlabeled cells were used as a reference to calculate relative increase or decrease in wide-field reflectance intensity.

3 RESULTS AND DISCUSSION

Transmission electron microscopy (TEM) images of gold, silver and gold-silver hybrid nanorods are shown in Fig. 2(a). The synthesis process is designed to yield rods with a length to diameter ratio of 50:10. For gold nanorods, the procedure results in uniformly shaped and relatively uniform sized nanoparticles. For silver nanorods, the TEM images illustrate the difficulty in controlling the size and shape of the particles resulting in heterogeneous structures that show the presence of spheres, triangles and rod-shaped particles of different sizes. This result highlights the difficulties associated with preparation of uniformly sized silver nanorods using current protocols. There is a need for a better understanding of various experimental factors such as pH, surfactants, and reducing agents to optimize the synthesis of silver nanorods. Despite the non-uniform shape of silver nanorods, we proceeded to evaluate the contrast properties of these nanorods. Homogeneous shape is not necessarily a prerequisite in all molecular imaging applications, provided the sizes of particles are within a desired range.

In order to combine the stability of gold nanorods with the higher scattering properties of silver nanorods, gold nanorods coated with silver was also synthesized. This technique produces relatively uniformly shaped Au-Ag nanorods compared to Ag nanorods. TEM images of this material show an increase in nanorod thickness after coating. We also observed a gradient in electron density between the gold and silver layers. However, some small spherical particles were also observed. It is likely that some of the small seeds (2-3 nm) of gold generated in the production of gold nanorods may have been enhanced by the deposition of silver, resulting in the formation of small spherical particles.

UV-Vis absorbance spectra of solutions of each type of nanoparticle are shown in Fig. 2(b). Gold nanorods show two distinct absorption peaks: a transverse peak at approximately 530 nm and a longitudinal peak at approximately 670 nm. Solutions of silver nanorods show two absorption peaks at approximately 430 nm and 575 nm. A solution of Au-Ag hybrid nanorods has peak absorption near 640 nm, slightly blue shifted relative to that of gold nanorods. We also observed a second absorption peak at approximately 430 nm corresponding to the absorption peak of silver. The spectral characteristics of hybrid nanorods can be explained by contributions from the silver coating on gold nanorods. Based on the absorbance values and the extinction coefficients of metal nanorods [13, 19], we estimated their concentration to be in the sub-nM range.

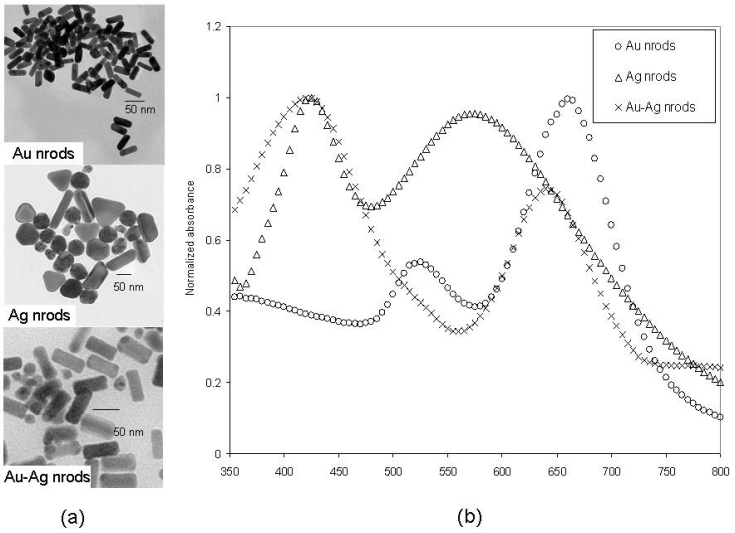

Fig. 2. (a) TEM images of Au, Ag, and Au-Ag hybrid nanorods and (b) corresponding UV-Vis spectra.

To assess the biocompatibility of the nanorods, we performed a standard viability study using the MTT assay. Metal nanoparticles coated with PSS polymer (concentration at sub-nM range) were incubated with cells in culture media for 24 h. The resulting cell viability was compared to untreated control cell samples. The normalized results for the biocompatibility study are shown in Fig 3. Results demonstrate that the PSS-coated nanorods of gold, silver and gold-silver hybrid nanorods are not cytotoxic to cells based on the standard MTT assay.

Fig. 4(a) illustrates the bioconjugation of targeting molecules such as anti-EGFR antibodies to PSS-coated nanorods. Antibodies are immobilized on the polyelectrolyte-coated nanorods using electrostatic interactions. Fig. 4(b) shows high-resolution confocal reflectance images of cells labeled with anti-EGFR coated gold, silver and gold-silver hybrid nanorods at 633 nm excitation. The results validate the specificity of molecular targeting of EGFR

expression in cancer cells. IgG-coated nanorods were used as a negative control to assess the level of non-specific interaction associated with these contrast agents.

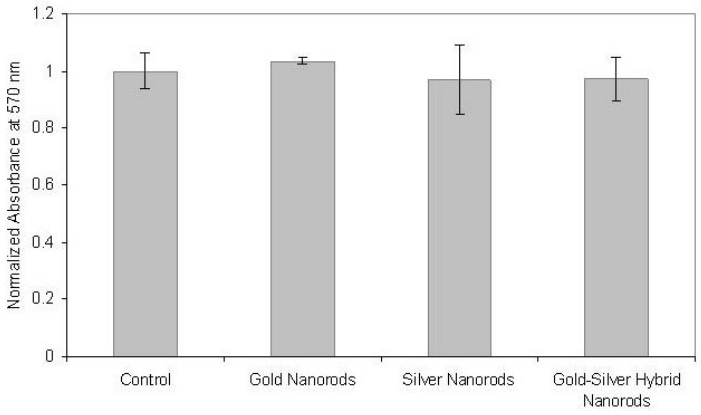

Fig. 3. Biocompatibility of PSS-coated nanorods based on the MTT assay.

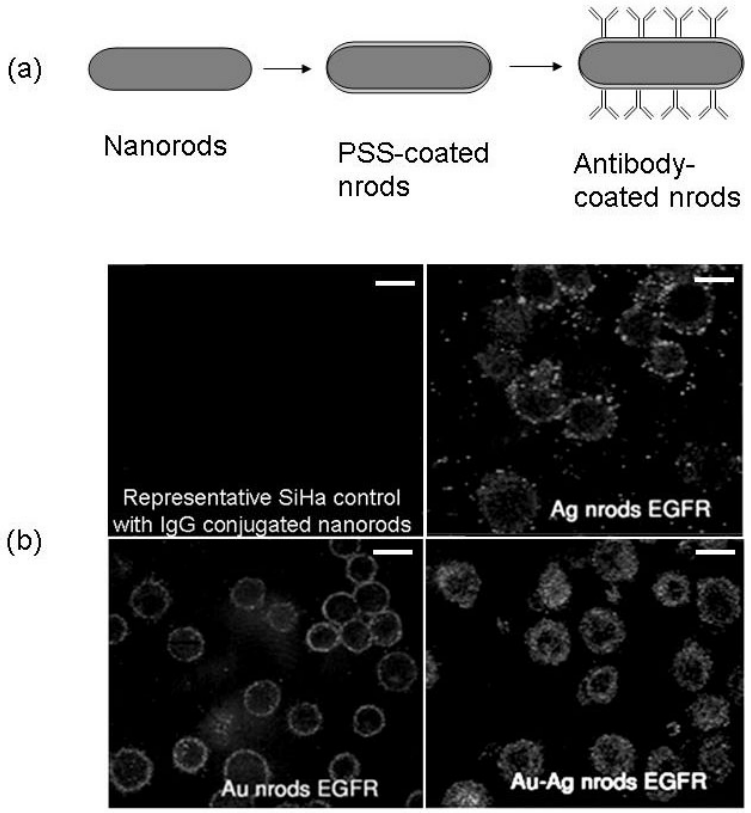

Fig. 4. (a) Schematic diagram of bioconjugation of antibodies to nanorods (b) and high-resolution confocal reflectance images of SiHa cells labeled with EGFR-targeted nanorods showing specific targeting of nanorod conjugates. Scale bar is 10 microns.

Next, we evaluated the optical contrast properties of these nanomaterials in various environments. Diffuse reflectance spectroscopy was used to predict the contrast properties of nanorods which could be achieved in wide-field imaging**.** Fig. 5 shows the diffuse reflectance spectra of gold, silver and gold-silver hybrid nanorods in various model phantoms. The reflectance measured from nanoparticles containing samples was normalized to the respective unlabeled background reflectance at each wavelength.

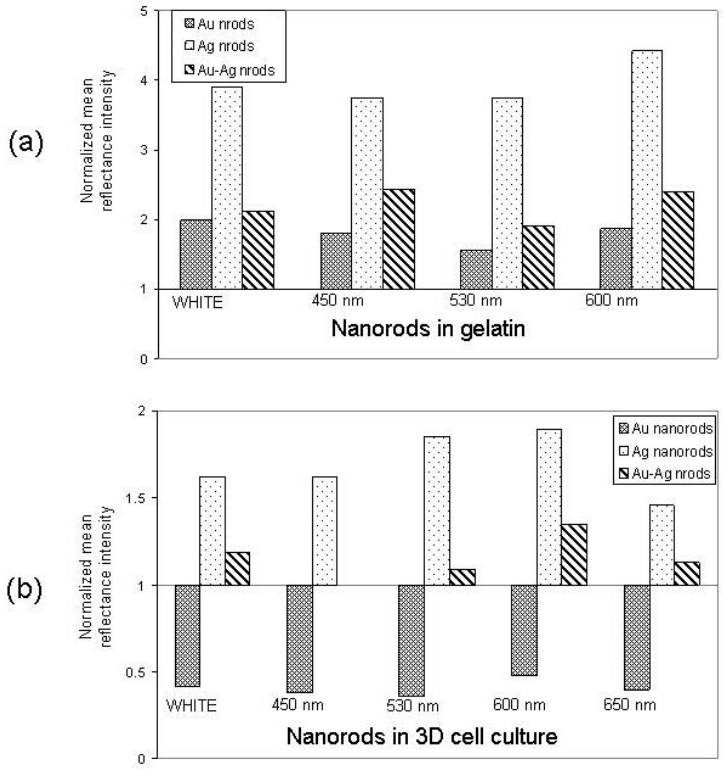

Fig. 5. Diffuse reflectance spectroscopy of (a) gold nanorods, (b) silver nanorods, and (c) gold-silver hybrid nanorods in water, gelatin, and 3D cell culture.

Fig. 5(a) shows diffuse reflectance spectra of gold nanorods in water, gelatin and 3D cell culture. The results show that the positive reflectance contrast decreases for gold nanorods as the background environment is changed from water to one which more closely resembles tissue. In water and gelatin phantoms, the peak contrast from gold nanorods is observed at the peak scattering wavelength of ~680 nm. Gold nanorods embedded in 3D cell culture also show a peak absorption contrast at ~530 nm, corresponding to the secondary transverse peak of gold nanorods in UV-Vis spectra. Fig. 5(b) shows the diffuse reflectance spectra of silver nanorods in different model systems. For silver nanorods, a broad diffuse scattering profile was observed with a peak around ~550 nm. This broadening of the scattering peak can be attributed to the heterogeneous population of anisotropic material as observed in the TEM analysis of silver nanorods. Silver nanorods also show a decrease in the positive contrast ratio

as the surrounding environment is changed to more closely resemble tissue. However, the positive contrast ratio of silver nanorods is 3-4-fold higher than that observed for gold nanoparticles under the same conditions. Despite the heterogeneity of silver nanorods, the resulting positive contrast is significantly higher than that of gold nanorods. To take advantage of the strong scattering of silver nanoparticles, we explored the use of gold-silver hybrid nanorods designed to combine the stability of gold nanorods with excellent contrast properties of silver nanorods. Fig. 5(c) shows the diffuse reflectance spectra of the gold-silver hybrid nanorods in different background environments. The gold-silver hybrid nanorods show an increase in positive contrast signal as compared to the gold nanorods. The results demonstrate that hybrid materials can improve the scattering contrast properties associated with gold nanorods.

Results of diffuse reflectance spectroscopy indicate that gold, silver, and gold-silver hybrid nanorods provide a higher positive contrast in dilute aqueous suspension than when suspended in the highly scattering environments of gelatin and 3D cell culture. The effective positive contrast ratio decreases as the scattering coefficient of the surrounding environment increases. We measured the scattering properties of the phantoms using the method described by Collier [20]. The scattering coefficient of gelatin phantoms was estimated to be ~6 cm^{-1} and for 3D cell culture was estimated to be 60 cm^{-1} at 830 nm. The scattering coefficient of the 3D cell culture is similar to that reported for cervical epithelium [21].

In order to evaluate whether the diffuse reflectance spectra of nanorods reported in Fig. 5 can accurately predict trends in image contrast achieved in wide-field imaging, we obtained wide-field reflectance images of nanorods in gelatin and 3D cell culture at several illumination wavelengths using a multi-spectral wide-field imaging system. Fig. 6(a) shows the average normalized reflectance intensity at various wavelengths for phantoms containing non-targeted metallic nanorods embedded in gelatin. The reflectance intensity values of phantoms containing non-targeted nanorods were normalized relative to an unlabeled gelatin phantom imaged under the same conditions. Results indicate that the contrast produced by silver nanorods is higher than that for both gold and gold-silver hybrid nanorods, consistent with the predictions of diffuse reflectance measurements in gelatin. Further, silver nanorods show a broad positive image contrast across the measured wavelength range, similar to the trends observed in diffuse reflectance measurements. In the case of hybrid nanorods, we observe a higher image contrast as compared to gold nanorods, consistent with the predictions of diffuse reflectance spectroscopy. Fig. 6(b) shows the average normalized reflectance intensity at various wavelengths of targeted metallic nanorods in 3D cell culture. The reflectance intensity values of phantoms containing molecular targeted contrast agents were normalized relative to unlabeled control 3D cell culture. The results indicate that gold nanorods predominantly produce absorptive contrast while silver and gold-silver hybrid nanorods produce positive scattering contrast when embedded in tissue-like environments. Again, the overall trend observed with wide-field imaging is in agreement with the results of diffuse reflectance spectroscopy. The results demonstrate that silver nanorods produce the greatest positive scattering contrast in wide-field imaging. The scattering signal of gold-silver hybrid nanorods is lower than that of silver nanorods but significantly higher than that of gold nanorods in all environments.

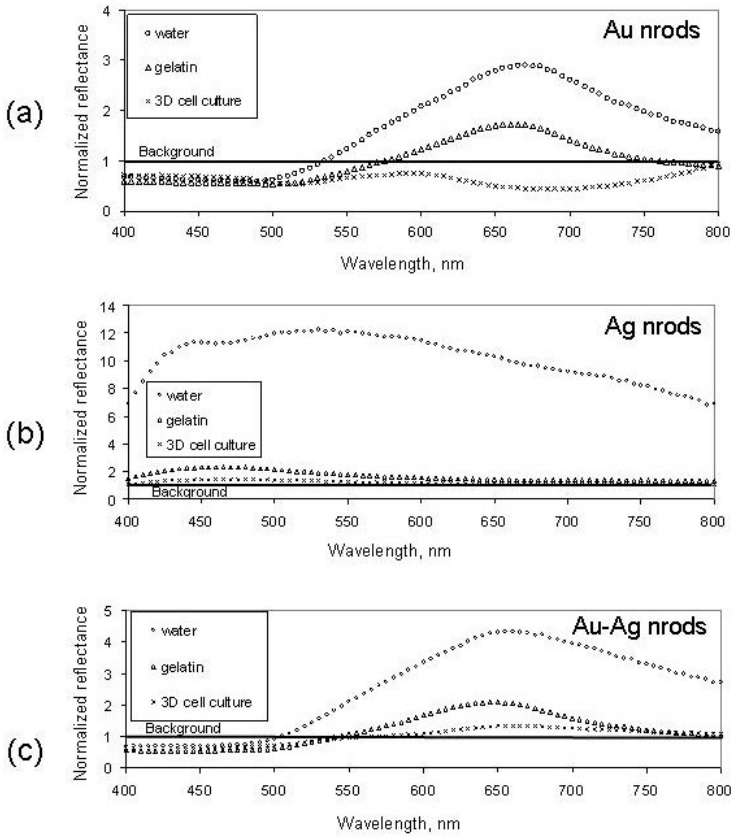

Fig. 6. Normalized mean reflectance intensity of (a) non-targeted nanorods in gelatin and (b) targeted nanorods in 3D cell culture. Intensity measurements are normalized to unlabeled controls.

4 CONCLUSION

We have demonstrated an approach to evaluate the effective image contrast of metal nanorods in biologically relevant environments. This study integrates diffuse spectroscopy to predict contrast properties and correlates the predictions with wide-field and high-resolution imaging to understand contrast properties as a function of size and composition of nanorods, imaging modality, presence of targeting molecules, and the surrounding environment.

As we increase the complexity of the surrounding media, we observe a decrease in the positive scattering contrast from nanorods. Silver-based nanorods offer higher scattering contrast compared to gold-based nanorods in different biological matrices; although synthesis of gold nanorods yields particles which are more homogeneous in size and shape than synthesis of silver nanorods. Engineering novel material compositions such as Au-Ag hybrid nanorods can be useful to develop contrast agents that are both homogeneous in size and shape and have high positive contrast properties.

Understanding the contrast properties of metal nanorods as a function of imaging conditions is an important step in designing molecule-specific contrast agents for optical molecular imaging. However, additional studies on the biocompatibility, delivery mechanisms, and clearance routes of these nanomaterials in biological tissues are necessary.

We are currently exploring these areas in order to develop an integrated approach in the clinical translation of these materials for biological imaging.

Acknowledgments

We thank Kenneth Dunner, Jr., and Cancer Center Core Grant CA16672 for TEM support, Vivian Mack for providing cell cultures, and BRP R01CA103830 NCI for funding. N. Nitin contributed equally to this manuscript.

References

[1] S. Eustis. and M.A. El-Sayed, "Why gold nanoparticles are more precious than pretty gold: Noble metal surface plasmon resonance and its enhancement of the radiative and nonradiative properties of nanocrystals of different shapes," *Chem. Soc. Rev.* **35**(3), 209-217 (2006). [doi:10.1039/b514191e].

[2] A.J. Haes, and R.P. Van Duyne, "A nanoscale optical biosensor: sensitivity and selectivity of an approach based on the localized surface plasmon resonance spectroscopy of triangular silver nanoparticles," *J. Am. Chem. Soc.* **124**(35), 10596-10604 (2002). [doi:10.1021/ja020393x].

[3] K. Sokolov, M. Follen, J. Aaron, I. Pavlova, A. Malpica, R. Lotan, and R. Richards-Kortum, "Real-time vital optical imaging of precancer using anti-epidermal growth factor receptor antibodies conjugated to gold nanoparticles," *Cancer Res.* **63**(9), 1999-2004 (2003).

[4] I.H. El-Sayed, X.H. Huang, and M.A. El-Sayed, "Surface plasmon resonance scattering and absorption of anti-EGFR antibody conjugated gold nanoparticles in cancer diagnostics: Applications in oral cancer," *Nano Lett.* **5**(5), 829-834 (2005). [doi:10.1021/nl050074e].

[5] N. Nitin, D.J. Javier, D.M. Roblyer, and R. Richards-Kortum, "Wide-field and high-resolution reflectance imaging of gold and silver nanospheres," *J. Biomed. Opt.* **12**(5), 051505/1-051505/10 (2007).

[6] Z. Cheng, J. Levi, Z. Xiong, O. Gheysens, S. Keren, X. Chen, and S.S. Gambhir, "Near-infrared fluorescent deoxyglucose analogue for tumor optical imaging in cell culture and living mice," *Bioconjugate Chem.* **17**(3), 662-669 (2006). [doi:10.1021/bc050345c].

[7] K.E. Adams, S. Ke, S. Kwon, F. Liang, Z. Fan, Y. Lu, K. Hirschi, M.E. Mawad, M.A. Barry, and E.M. Sevick-Muraca, "Comparison of visible and near-infrared wavelength-excitable fluorescent dyes for molecular imaging of cancer," *J. Biomed. Opt.* **12**(2), 024017/1-024017/9 (2007).

[8] J.W. Chen, S.M. Querol, A. Bagdanov Jr., and R. Weissleder, "Imaging of myeloperoxidase in mice by using novel amplifiable paramagnetic substrates," *Radiol.* **240**(2), 473-81 (2006). [doi:10.1148/radiol.2402050994].

[9] P.K. Jain, K.S. Lee, I.H. El-Sayed, and M.A. El-Sayed, "Calculated absorption and scattering properties of gold nanoparticles of different size, shape, and composition: applications in biological imaging and biomedicine," *J. Phys. Chem. B* **110**(14), 7238-7248 (2006). [doi:10.1021/jp057170o].

[10] C.J. Murphy, T.K. Sau, A.M. Gole, C.J. Orendorff, J. Gao, L. Gou, S.E. Hunyadi, and T. Li, "Anisotropic metal nanoparticles: synthesis, assembly, and optical applications," *J .Phys. Chem. B* **109**(29), 13857-13870 (2005). [doi:10.1021/jp0516846].

[11] C. Yu, L. Varghese, and J. Irudayaraj, "Surface modification of cetyltrimethylammonium bromide-capped gold nanorods to make molecular probes," *Langmuir* **23**(17), 9114-9119 (2007). [doi:10.1021/la701111e].

[12] D.I. Gittins, and F. Caruso, "Tailoring the polyelectrolyte coating of metal nanoparticles," *J. Phys. Chem. B* **105**(29), 6846-6852 (2001). [doi:10.1021/jp0111665].
[13] H. Liao, and J.H. Hafner, "Gold nanorod bioconjugates," *Chem. Mater.* **17**(18), 4636-4641 (2005). [doi:10.1021/cm050935k].
[14] B. Nikoobakht, and M.A. El-Sayed, "Preparation and growth mechanism of gold nanorods (NRs) using seed-mediated growth method," *Chem. Mater.* **15**(10), 1957-1962 (2003). [doi:10.1021/cm020732l].
[15] N.R. Jana, L. Gearheart, and C.J. Murphy, "Wet chemical synthesis of silver nanorods and nanowires of controllable aspect ratio," *Chem. Commun.* **7,** 617-618 (2001). [doi:10.1039/b100521i]
[16] M.Z. Liu, and P. Guyot-Sionnest, "Synthesis and optical characterization of Au/Ag core/shell nanorods," *J. Phys. Chem. B* **108**(19), 5882-5888 (2004). [doi:10.1021/jp037644o]
[17] A. Gole, and C.J. Murphy, "Polyelectrolyte-coated gold nanorods: synthesis, characterization and immobilization," *Chem. Mater.* **17**(6), 1325-1330 (2005). [doi:10.1021/cm048297d].
[18] D.M. Roblyer, C. Kurachi,, K. Sokolov, A.K. El-Naggar, M.D. Williams, A.M. Gillenwater, and R. Richards-Kortum," A multispectral optical imaging device for in vivo detection of oral neoplasia," *J. Biomed. Opt.* in press. (Mar/Apr 2008 issue).
[19] C.J. Orendorff, and C.J. Murphy, "Quantitation of metal content in the silver-assisted growth of gold nanorods," *J. Phys. Chem. B* **110**(9), 3990-3994 (2006). [doi:10.1021/jp0570972].
[20] T. Collier, M. Follen, A. Malpica, and R. Richards-Kortum, "Sources of scattering in cervical tissue: determination of the scattering coefficient by confocal microscopy," *Appl. Opt.* **44**(11), 2072-81 (2005). [doi:10.1364/AO.44.002072].
[21] T. Collier, D. Arifler, A. Malpica, M. Follen, and R. Richards-Kortum, "Determination of epithelial tissue scattering coefficient using confocal microscopy," *IEEE J. Sel. Top. Quantum Electron.* **9**(2), 307-313 (2003). [doi:10.1109/JSTQE.2003.814413].